International Journal of Rock Mechanics & Mining Sciences ▮ (▮▮▮▮) ▮▮▮–▮▮▮

Contents lists available at ScienceDirect

International Journal of Rock Mechanics & Mining Sciences

journal homepage: www.elsevier.com/locate/ijrmms

Hydro-mechanical modelling of the excavation damaged zone around an underground excavation at Mont Terri Rock Laboratory

Séverine Levasseur [a,b,*], Robert Charlier [a], Bernd Frieg [c], Frédéric Collin [a,b]

[a] Université de Liège, Department ArGEnCo, Chemin des Chevreuils 1, 4000 Liège 1, Belgium
[b] FRS-FNRS – Fonds National de la Recherche Scientifique, rue d'Egmont 5, B-1000 Bruxelles, Belgium
[c] NAGRA, National Cooperative for the Disposal of Radioactive Waste in Switzerland, Hardstrasse 73, 5430 Wettingen, Switzerland

ARTICLE INFO

Article history:
Received 12 June 2009
Received in revised form
29 December 2009
Accepted 8 January 2010

Keywords:
Hydro-mechanical coupling
Fracturing
Permeability tensor
Underground excavation
Indurated clay
Finite element method

ABSTRACT

A zone with significant irreversible deformations and significant changes in flow and transport properties is expected to be formed around underground excavations in indurated clay. The stress perturbation around the excavation could lead to a significant increase of the permeability, related to diffuse and/or localised crack propagation in the material. The main objective of this study is to model these processes at large scale in order to assess their impacts on the performance of radioactive waste geological repositories. This paper concerns particularly the hydro-mechanical modelling of a long-term dilatometer experiment performed in Mont Terri Rock Laboratory in Switzerland. The proposed model defines the permeability as a function of the aperture of the cracks that are generated during the excavation. With this model, the permeability tensor becomes anisotropic. Advantages and drawbacks of this approach are described using the results of the Selfrac long-term dilatometer experiment.

1. Introduction

The excavation process creates a perturbed zone around underground structure openings in rock masses, where geotechnical and hydro-geological properties are altered. According to the degree of perturbation, this zone can be divided into two parts: the excavation disturbed zone (EdZ) and the excavation damaged zone (EDZ). The creation of these excavation disturbed and damaged zones are expected for all geological formations. In the context of radioactive waste disposal, Tsang et al. [1] suggest defining the EdZ as a zone with hydro-mechanical and geo-chemical modifications, without major changes in flow and transport properties, and the EDZ as a zone in which hydro-mechanical and geo-chemical modifications induce significant changes in flow and transport properties, resulting to macro and micro-fracturing and a rearrangement of rock structures. These changes can include one or more orders of magnitude increase in flow permeability. Then, as the potential host rocks must be characterised by a very low hydraulic conductivity [2,3], it means that EDZ has the main implications for the operation and long-term performance of underground nuclear waste repository. Behaviour of this zone is mainly considered in this paper; illustration focuses only on the indurated Opalinus Clay of the Mont Terri underground research laboratory in Switzerland.

The general hydro-mechanical behaviour of this overconsolidated clay depends mainly on the stress history, the stiffness, the strength and its undisturbed structure, but it is also influenced by the presence and the orientation of discontinuities or micro-cracks, which result in elastic stiffness reduction and variations of permeability. For Opalinus clay, Bernier et al. [4] explain that if natural fractures induce in general no significant increase in hydraulic parameters compare to intact rock (as long as the effective stress normal to the fracture planes exceeds a certain threshold value), perturbations caused by an excavation may lead to a significant increase of the permeability related to diffuse and/or localised crack proliferation in the EDZ of the material. The structure of this EDZ is controlled by the stress field and the anisotropy of the Opalinus Clay. For tunnels constructed parallel to bedding, extensional features due to unloading dominate the EDZ in the side walls, while the deformation in the roof and floor is controlled by strength of the bedding planes. A combination of shear and extensional failure characterises this area. Then, as within the EDZ the permeability may increase by several orders of magnitude, the implication of a higher diffusive and advective properties and its time evolution according to various repository safety scenarios need to be evaluated as a part of the repository safety assessments [1,5]. Various issues need to be part of the

* Corresponding author at: Université de Liège, Department ArGEnCo, Chemin des Chevreuils 1, 4000 Liège 1, Belgium. Tel.: +32 4 366 91 43; fax: +32 4 366 93 26.
E-mail address: severine.levasseur@ulg.ac.be (S. Levasseur).

1365-1609/$ - see front matter © 2010 Elsevier Ltd. All rights reserved.
doi:10.1016/j.ijrmms.2010.01.006

evaluation, such as processes creating fractures in the excavation damaged zone, the order of magnitude of permeability increase, potential for sealing or healing (with permeability reduction) in the zone.

Then to better understand and quantify fracturing and sealing processes in clays, the Selfrac project [5] was undertaken within the 5th EURATOM Framework Programme (1998–2002). Laboratory tests, in situ experiments and models were developed for Opalinus Clay and Boom Clay to understand and to quantify hydro-mechanical behaviour of the engineered barrier system in these geological formations and to assess their impacts on the performance of radioactive waste geological repositories in order to improve the geo-structure design. In this paper, we propose to revisit the long-term dilatometer experiment performed in Opalinus Clay at the Mont Terri Underground Research Laboratory in Switzerland, and to propose a hydro-mechanical model able to reproduce the evolution of permeability in the EDZ of Opalinus Clay during the sealing process. In this model, evolution of the permeability within the EDZ is associated with discontinuities, represented by strain localisation or damage [4]. In fact, when a rock is damaged, crack networks are created, which could constitute preferential flow paths, depending on crack interaction. As a consequence, the rock hydraulic conductivity increases and can become heterogeneous and anisotropic [6]. The permeability of crack is usually related to the crack aperture [7] and the key issue is thus to propose a model providing the relationship between rock mass permeability and crack aperture, as well as the evolution of the crack aperture during the excavation. Different approaches exist to tackle this problem, from micro–macro theories [8] to macroscopic (phenomenological) ones [9,10]. In this paper, we use the latter to relate the aperture evolution to the strain tensor [11,12]. Geo-chemical effects, which could act on crack characteristics and then on the permeability evolution in EDZ, are neglected. As a starting point of our development, we describe first, in Section 2, the long-term dilatometer experiment, which is supposed to simulate the bentonite swelling pressure and to exhibit its influence with time on the transmissivity of the Excavation Damaged Zone in a direction parallel to the borehole axes (axial transmissivity). The proposed developments on the permeability evolution are presented in Section 3, as well as the improvements of the finite element formulation. In the Section 4, a numerical study on the hydro-mechanical coupled effect in the EDZ observed in the Selfrac experiment is proposed. Some comparisons with the experimental results show that this phenomenological approach permits to reasonably reproduce the behaviours observed in situ, like the decrease of the hydraulic conductivity in the EDZ with the dilatometer pressure increase. Finally, some conclusions and further perspectives of this study are given in Section 5.

2. Selfrac project

The Selfrac project aimed to understand and to quantify the EDZ fracturing in clay and its evolution with time (sealing process) in order to assess its impact on the performances of radioactive waste geological repositories. Two different potential geological formations for deep radioactive waste repositories were investigated: the indurated Opalinus Clay in Switzerland and the plastic Boom Clay in Belgium. This paper only concerns the long-term dilatometer experiment performed in Opalinus Clay. The general concept of this experiment was to combine dilatometer tests and numerous hydraulic tests with multi-packer system to test the influence of bentonite swelling pressure on the axial transmissivity of the Excavation Damaged Zone (EDZ) [4,13]. The pressure in the dilatometer probe, which has modelled the effect of the bentonite swelling pressure, was increased stepwise and hydraulic tests were periodically performed under different dilatometer pressures. Active hydraulic tests were carried out periodically in the deepest interval of the borehole. The pressure responses were observed in the test interval as well as in the interval above the dilatometer. It can be assumed that pressure changes were preferably transmitted through the EDZ along the borehole. So, the problem was to know if the inflation pressure of the dilatometer can influence flows in EDZ. Then, by modelling this experiment, our main objective in this paper is to check if the hydraulic conductivity of the EDZ can be seen as a function of the dilatometer pressure.

2.1. Opalinus clay

Located in the Jura Mountains of the north-western Switzerland, Mont Terri site is an asymmetrical anticline folded during the Late Miocene to Pilocene period. The rock laboratory is located within the Opalinus Clay unit which is a Jurassic deposit consisting of a sequence of overconsolidated claystones and marls and has a dip of approximately 45° southeast [14,15]. This clay exhibits at its natural state very favourable conditions for the disposal of radioactive wastes thanks to low and uniform hydraulic conductivity, low diffusion coefficients and good retention capacity for radionuclides [3]. This clay rock can be characterized as a stiff overconsolidated clay with a hydraulic conductivity of about $2\times10^{-20}\,m^2$, a Young's modulus between 4 and 10 GPa and a cohesion higher than 2 MPa [16].

One concern regarding nuclear waste disposal is that the generally favourable properties of such formations could change and the host rock could loose part of its barrier function due to the disturbance and damage in the vicinity of the repository that result from the necessary excavations. Behaviour of indurated clays is brittle and then fractures are quite common in such materials. Field observations on indurated clays show that the EDZ contains two sets of fractures and micro-fractures induced by excavation in the perpendicular direction to the strike of bedding. These fractures can be of extensional or shear origin. One of the set is oriented sub-parallel with the tunnel axis in the sidewalls and corresponds to open unloading joints while the other is oriented sub-parallel with bedding and corresponds to reactivated bedding planes [17]. However, according to Corkum and Martin [15], as Opalinus clay mineralogy consists mainly of kaolinite and illite, yield is mainly caused by tension. Then, most fractures in the EDZ in indurated clays are directly caused by unloading induced by the short-term excavation (undrained elasto-plastic response) and are of extensional nature [18,19]. According to Bossart et al. [20], EDZ shape around spherical excavation is slightly elliptical with vertical long axis and extends for 0.5–1 tunnel radii from the excavation periphery.

2.2. Long-term dilatometer experiment design

Fig. 1a presents the general design of the Selfrac Experiment. From the gallery of the Mont Terri rock laboratory, a new borehole, named BSE-3, is drilled (Fig. 1b) by air circulation. In this borehole of 12.1 m (11.9 m of Opalinus Clay and 0.2 m of concrete), a dilatometer probe (packer length 1 m, diameter 10 cm) is installed and combined with two inflatable packers in a single test string. The dilatometer is positioned at the lowest part of the multi-packer system. Therefore, it is placed into the bottom part of the borehole after installation of the equipment. The dilatometer acts as a normal hydraulic packer element, which can be set with different inflation pressure and isolates

Please cite this article as: Levasseur S, et al. Hydro-mechanical modelling of the excavation damaged zone around an underground excavation at Mont Terri Rock Laboratory. Int J Rock Mech Mining Sci (2010), doi:10.1016/j.ijrmms.2010.01.006

hydraulically the bottom section (I1 = 2.88 m) of the borehole from the upper ones. A high pressure packer with a sealing length of 1.5 m (to minimize the risk of packer by-pass) isolates a second test interval (I2 = 1.02 m) above the dilatometer. The static pressure difference between the bottom interval (I1) and interval I2 is expected to be quite low because they have nearly the same distance from the tunnel wall and therefore comparable positions in the rock mass. In addition, the two intervals are separated by the dilatometer of 1 m length only. The third packer (sealing length 1 m) is a "guard packer" to ensure stable conditions in the upper part of the borehole (interval I3 = 2.68 m) and also to measure the pressure build-up and the influence of the tunnel on the formation pressure. Active hydraulic tests are carried out periodically in the deepest interval (I1). The pressure reactions are observed in the test interval itself as well as in the intervals above the dilatometer. More details on this experiment can be found in [4,13].

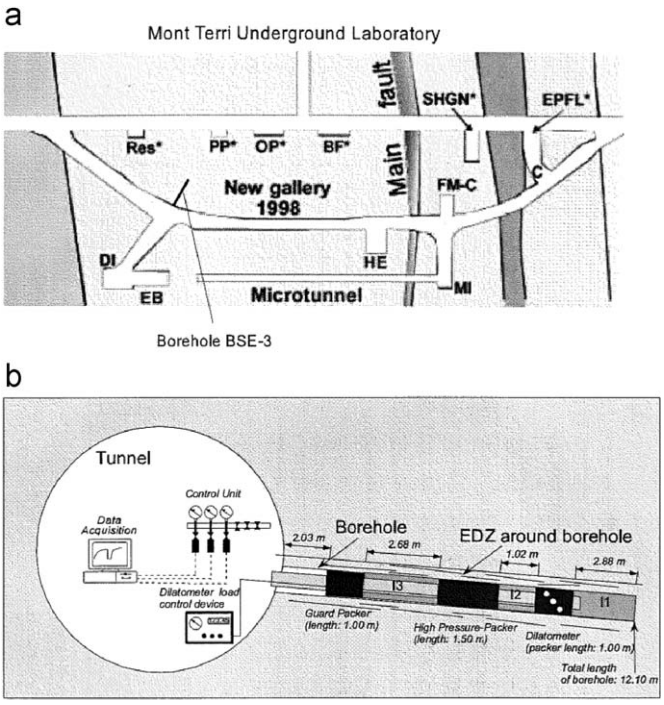

Fig. 1. Long-term dilatometer experiment: (a) location in Mont Terri Underground Laboratory of the Borehole BSE-3 and (b) experiment layout [14].

2.3. Loadings and hydraulic tests during the long-term dilatometer experiment

The pressure in the dilatometer probe is increased stepwise to 5 MPa and hydraulic tests are periodically performed under different dilatometer pressures. Constant rate injection, pulse injection or pulse withdrawal tests are carried out periodically in the deepest interval (I1) following the chronological overview presented in Table 1. Constant rate injection tests consist of fluid injection in interval I1 with a constant rate during a defined period (several hours). Pulse tests consist of injection or pumping of fluid in the interval 1 (I1) during a short period (few seconds).

Fig. 2 summarizes the experiment process. It represents the evolution with time of the dilatometer pressure and the water pressures measured in intervals I1, I2 and I3. This figure confirms that water pressure in interval I3 is quite constant with dilatometer pressure during all the experiment. The packers well isolate the deepest part of the borehole, where experiment takes place, to the gallery. Concerning I1 and I2 water pressure evolutions during the experiment, Fig. 2 seems to show that these pressures evolved separately with the increase of dilatometer load. To better see this phenomenon, results of Fig. 2 can be translated into Fig. 3 which represents the ratio between I1 and I2 pressure increments with dilatometer pressure. These both figures illustrate the fact that the early hydraulic tests (period A), realised in interval I1, provide fast pressure reactions in the I2 neighbouring interval between the dilatometer and the central packer. Pressure ratio in Fig. 3 is small and quite independent to the dilatometer load. This could be characteristic of hydraulic connexion between I1 and I2. Since the dilatometer pressure is less than about 3.5 MPa, the contact between dilatometer and clay is not tight and water can flow along the dilatometer from I1 to I2. However, as far as the dilatometer pressure increases (>3.5 MPa, period B), the pressure in I1 increases with the dilatometer load whereas pressure in I2 increasing is less significant. Moreover, I2 time of reaction to the pressure modification in I1 reduced with the dilatometer load. It results that the pressure ratio in Fig. 3 strongly increases with the dilatometer load. This could be characteristic of a hydraulic separation of the two intervals above and below the dilatometer. The contact between dilatometer probe and clay is tight. I1 and I2 intervals are hydraulically uncoupled. Finally, when the dilatometer pressure is larger than 3.5 MPa, it could be assumed that the transmissivity decreases with the increase of dilatometer load on the borehole. This is the consequence of the microcraks closure in the EDZ due to the dilatometer load. This led to the conclusion that inflation pressure of the dilatometer influence flows in EDZ, the hydraulic

Table 1
Chronological overview of the main activities.

Event	Date	Activity	
1	T_0	Installation of dilatometer and packers	
2	T_0+10 hours	Increase pressure of dilatometer and packers	Pressure = 3.0 MPa
3	T_0+48 days	Constant rate injection test	Injection of 0.83 ml/min during 3 h45
4	T_0+90 days	Pulse injection test	Injection of 39 ml during 35 s
5	T_0+91 days	Increase pressure of dilatometer	Pressure = 3.5 MPa
6	T_0+125 days	Constant rate injection test	Injection of 0.02 ml/min during 102 min and 0.1 ml/min during 21 h38 min
7	T_0+127 days	Increase pressure of dilatometer	Pressure = 4.0 MPa
8	T_0+146 days	Pulse withdrawal test	Pumping of 32 ml during 9 s
9	T_0+148 days	Increase pressure of dilatometer	Pressure = 4.5 MPa
10	T_0+174 days	Pulse withdrawal test	Pumping of 30.5 ml during 17 s
11	T_0+240 days	Increase pressure of dilatometer	Pressure = 5.0 MPa
12	T_0+257 days	Pulse withdrawal test	Pumping of 33.5 ml during 61 s
13	T_0+304 days	Pulse withdrawal test	Pumping of 34 ml during 26 s

Please cite this article as: Levasseur S, et al. Hydro-mechanical modelling of the excavation damaged zone around an underground excavation at Mont Terri Rock Laboratory. Int J Rock Mech Mining Sci (2010), doi:10.1016/j.ijrmms.2010.01.006

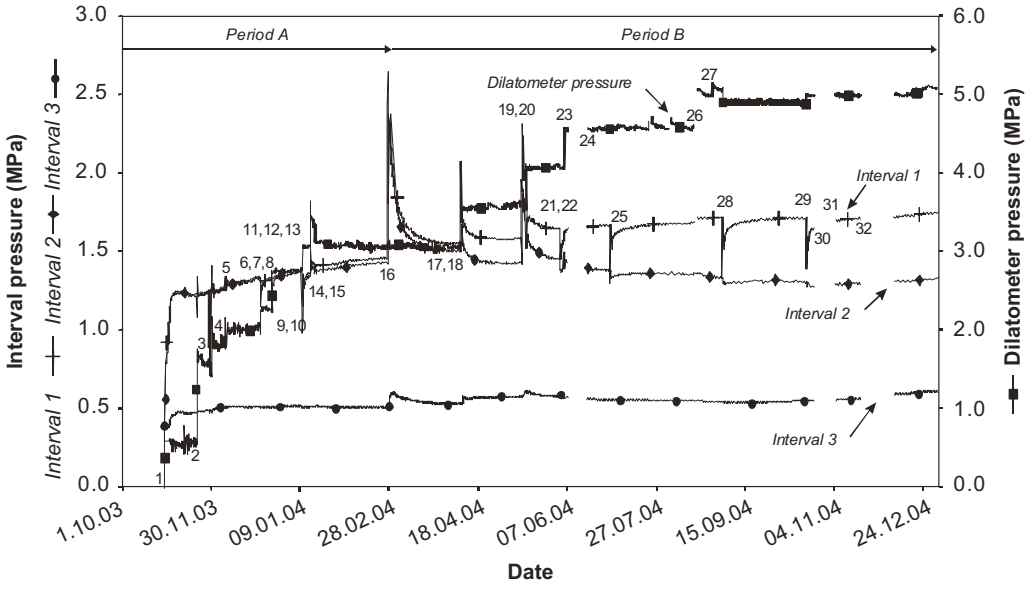

Fig. 2. Overview of the project progress [14].

conductivity of the EDZ can be seen as a function of the dilatometer pressure [4].

3. Hydro-mechanically coupled modelling and permeability evolution in EDZ

A zone with higher transmissivity along the borehole, corresponding to the EDZ in the direct vicinity of the tunnel, is formed after drilling of the borehole due to the stress release and stress redistribution. The appearance of this latter redistribution closed to the underground excavation leads to anisotropic permeability changes around this construction. Insofar as the low permeability is one of the desired properties for the host formation, all the processes influencing this diffusion property need to be understood and evaluated. In the literature, most of the studies concerning this topic propose to link the permeability tensor to stress or strain tensors. These developments are generally performed at the rock joint scale. The objective of this paper is to extend these local scale models to larger scale in order to describe the global hydro-mechanical behaviour in EDZ around tunnels.

3.1. A brief overview of permeability evolution models

When a localised fracture is generated by tension in indurated clay, a huge increase in hydraulic conductivity is experimentally noticed [1,4]. This evolution of the permeability with deformations can be directly associated with strain localisation or damage. When a rock is damaged, crack networks are created, that are favourable to water flow. As a consequence, the rock hydraulic conductivity increases because of cracks and the permeability tensor becomes heterogeneous and anisotropic. To explain this phenomenon, analytical relations between hydraulic conductivity and crack opening or between hydraulic conductivity and normal stress are proposed in literature [9,21]. Traditionally, fluid flow through rock joints has been described by the cubic law, which follows the assumption that joints consist of two smooth parallel plates [22]. However, experimental studies on real fractures [23,24] show that the relation between stress and hydraulic conductivity is not so simple. Real rock joints have rough walls

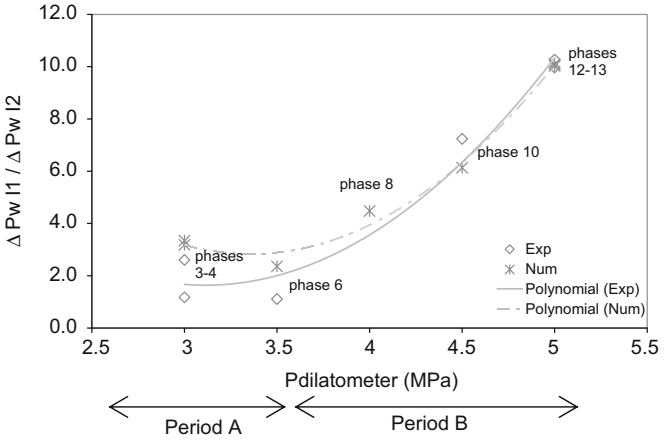

Fig. 3. Ratio of water pressure modifications in I1 and I2 intervals and polynomial tendency curves versus dilatometer loading: comparison between in-situ measurements (◇) and numerical responses (*).

and variable apertures, as well as asperity areas where the two opposed surfaces of the joint walls are in contact with each other. All these characteristics perturb flow in rock joints and make the cubic law, in its classic form, inappropriate. Then, to improve the fluid flow formulation, authors often propose in literature to weight the crack opening effect with a more or less sophisticate coefficient. Based on rock joint observations, most of the authors introduce micro- or macro-roughness coefficients (JRC) or hydraulic aperture coefficients [10,25,26]. Some others prefer to take into account the crack network geometry, the effective normal stress and the shear displacement as well as a set of parameters characterizing the behaviour of the fracture (i.e. the roughness coefficient JRC and the compressive strength of fracture JCS) [12]. But the cubic law can also be transformed by weight coefficients characterizing the rock quality, like a modulus reduction ratio [11], or the flow dissipation energy [27]. In this latter method, the coupling effect between fluid flow and deformation is considered through the connectivity impact of the fracture network on fluid flow. All these methods are interesting to characterize fluid flow in cracked media.

Please cite this article as: Levasseur S, et al. Hydro-mechanical modelling of the excavation damaged zone around an underground excavation at Mont Terri Rock Laboratory. Int J Rock Mech Mining Sci (2010), doi:10.1016/j.ijrmms.2010.01.006

Unfortunately, they have been defined for particular loading conditions at joint scale. Their extension to larger problems (tunnel/borehole drilling) needs to be realised with caution.

For Opalinus Clay, a significant permeability variation is associated with a discontinuity at sample scale and not with diffuse damage as observed for other rocks like salt or granite [4]. At the tunnel scale, most discrete features in the EDZ are caused directly by the short-term excavation-induced unloading (undrained elasto-plastic response) and are of extensional nature. Considering these assumptions, we propose thus in the following section to extend the previous models (developed at the joint scale) to the estimation of the permeability evolution in the EDZ, where some discrete fracture networks are created. The cubic law weight coefficient is chosen as a non-dimensional coefficient A, calibrated on experimental data. This one is supposed to merge averaged characteristics and behaviours of rock joints all along the borehole.

3.2. Permeability tensor evolution with strain

Schematically, a crack can be seen as two parallel plates or a flat ellipsoid, like illustrated in Fig. 4. The flow modelling in this crack is considered in equivalent Darcy's media, in which the permeability value (in meter square, m^2) parallel to the crack plane (noted t on Fig. 4a) is estimated by Poiseuille's solution:

$$k^{cr} = \frac{\lambda b^2}{12} \tag{1}$$

in which b corresponds to the crack width (in meter) and λ is a roughness coefficient (without dimension) equal to one for an ideal flow and less than one when the head decrease because of crack roughness.

The permeability k_m of a medium with one set of cracks (Fig. 4b) can also be related to the ratio between the width b of cracks and the crack spacing B (in meter) [9,11]:

$$k_m = \lambda \frac{b^3}{12B} \tag{2}$$

where k_m is the permeability in the crack direction (in m^2). Considering a general formulation in (e_1,e_2) axes, the permeability tensor becomes:

$$k_{ij} = \lambda \frac{b^3}{12B}[\delta_{ij} - n_i n_j] \tag{3}$$

with $\underline{n} = [n_1 \ n_2]_{(e_1,e_2)} = [-\sin\alpha_n \ \cos\alpha_n]_{(e_1,e_2)}$ being the normal of the cracks.

During excavation or borehole drilling, localised fractures are generated in the medium due to the stress release and stress redistribution. In this model, crack spacing B is assumed to remain constant while crack width b is assumed to evolve as: $b = b_0 + \Delta b$, with b_0 the initial width and Δb the crack opening. Then, Eq. (3) becomes

$$k_{ij} = \frac{\lambda}{12B}[b_0 + \Delta b]^3[\delta_{ij} - n_i n_j] \tag{4}$$

$$k_{ij} = \frac{\lambda b_0^3}{12B}[1 + \Delta b/b_0]^3[\delta_{ij} - n_i n_j] \tag{5}$$

in which the initial permeability in crack direction is equal to $k^0 = (\lambda b_0^3/12B)$ (m^2).

Localised fractures are mainly generated by tension in Opalinus Clay. The crack opening over the initial width is assumed to be a linear function of tensile strain ε^T in the normal direction of the crack [11,12]: $\Delta b/b_0 = A\varepsilon^T$, with A, a non-dimensional weight coefficient which concentrates the crack properties, then:

$$k_{ij} = k^0[1 + A\varepsilon^T]^3[\delta_{ij} - n_i n_j] \tag{6}$$

This expression can be generalized for a medium with orthogonal sets of cracks oriented parallel to the principle strain directions. Following [11], the global permeability tensor (in m^2) of the medium corresponds to the sum of the contributions of each n-crack:

$$k_{ij} = \sum_{n=1}^{2} k_n^0 (1 + A_n \varepsilon_n^T)^3 \beta_{ij}(\alpha_n) \tag{7}$$

with $k_n{}^0$ being the initial permeability in the direction of the n-crack (in m^2),

$$\varepsilon_n^T = \langle \varepsilon_n \rangle = \begin{cases} 0 & \text{if } \varepsilon_n \le 0 \\ \varepsilon & \text{if } \varepsilon_n > 0 \end{cases}$$

with ε_n the strain in the normal direction of the n-crack, A_n the weight coefficient associated with the n-crack properties (dimensionless),

$$\beta_{ij}(\alpha_n) = \begin{pmatrix} 1-\sin^2\alpha_n & \cos\alpha_n \sin\alpha_n \\ \cos\alpha_n \sin\alpha_n & 1-\cos^2\alpha_n \end{pmatrix}_{(e_1,e_2)}$$

α_n the orientation of cracks, which is assumed to follow the orientation of the principle strain directions,

$$\alpha_n = \frac{1}{2} arctg\left(\frac{2\varepsilon_{12}}{\varepsilon_{11} - \varepsilon_{22}}\right) + (n-2)\frac{\pi}{2} \quad \text{with } n = 1, 2.$$

In expression (7), permeability tensor is calculated from the total strain (at each Gauss point of a finite element model) relying on the assumption of a constant strain tensor orientation. However, during the loading history of a general problem, the strain orientation may change and this latter assumption is no more valid. The permeability tensor may thus be expressed as a function of the strain increment and strain orientation variation as follows:

$$k_{ij} = k_{ij} + \Delta k_{ij} \tag{8}$$

with

$$\Delta k_{ij} = \frac{\partial k_{ij}}{\partial \varepsilon_n} \Delta \varepsilon_n^T + \frac{\partial k_{ij}}{\partial \alpha_n} \Delta \alpha_n$$

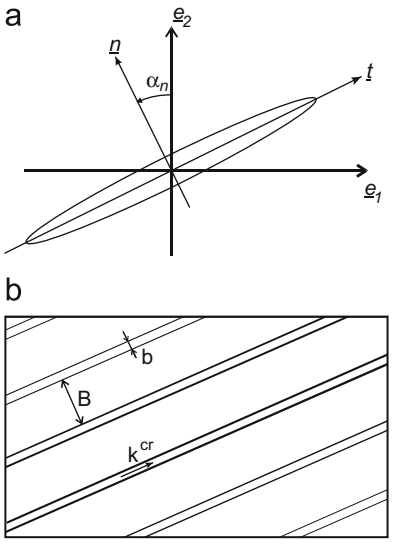

Fig. 4. Schematic representation of crack by an oriented ellipsoid (a), by parallel plates (b).

Please cite this article as: Levasseur S, et al. Hydro-mechanical modelling of the excavation damaged zone around an underground excavation at Mont Terri Rock Laboratory. Int J Rock Mech Mining Sci (2010), doi:10.1016/j.ijrmms.2010.01.006

and

$$\frac{\partial k_{ij}}{\partial \varepsilon_n} = 3A_n k_n^0 (1+A_n \varepsilon_n^T)^2 \beta_{ij}(\alpha_n)$$

$$\frac{\partial k_{ij}}{\partial \alpha_n} = k_n^0 (1+A_n \varepsilon_n^T)^3 \gamma_{ij}(\alpha_n)$$

in which

$$\gamma_{ij}(\alpha_n) = \frac{\partial \beta_{ij}}{\partial \alpha_n} = \begin{pmatrix} -2\cos\alpha_n \sin\alpha_n & \cos^2\alpha_n - \sin^2\alpha_n \\ \cos^2\alpha_n - \sin^2\alpha_n & 2\cos\alpha_n \sin\alpha_n \end{pmatrix}$$

3.3. Hydro-mechanical finite element formulation

The governing equations for a coupled hydro-mechanical problem are restricted to two equations in case of quasi-static conditions in a saturated porous media. Following the ideas of Lewis and Schrefler [28], these equations are the mixture (solid skeleton and fluid phase) balance of momentum equation and the water mass balance equation. In the following developments, the balance equations are written in the current solid configuration denoted Ω^t (updated Lagrangian formulation).

In the mixture balance of momentum equation, the interaction forces between fluid phases and grain skeleton cancels. In a weak form (virtual work principle), this equation reads for any kinematically admissible virtual displacement field u_i^*:

$$\int_{\Omega^t} \sigma_{ij}^t \varepsilon_{ij}^* \, d\Omega^t = \int_{\Omega^t} (\rho_s(1-\phi^t) + \rho_w^t \phi^t) g_i u_i^* \, d\Omega^t + \int_{\Gamma_\sigma^t} \bar{t}_i^t u_i^* \, d\Gamma^t \tag{9}$$

where $\varepsilon_{ij}^* = (1/2)(\partial u_i^*/\partial x_j^t + \partial u_j^*/\partial x_i^t)$ is the kinematically admissible virtual strain field, ϕ^t is the porosity defined as $\phi^t = \Omega^{v,t}/\Omega^t$, where Ω^t is the current volume of a given mass of skeleton and $\Omega^{v,t}$ the corresponding porous volume, ρ_s is the solid grain density, ρ_w^t is the water density, g_i is the gravity acceleration and Γ_σ^t is the part of the boundary where tensions $\bar{t}_i^t$ are known.

The total stress σ_{ij}^t is defined as a function of the kinematics. Here we assume first the Terzhagi's definition of effective stress:

$$\sigma_{ij}^t = \sigma'^t_{ij} - p_w^t \delta_{ij} \tag{10}$$

with σ'^t_{ij} the effective stress and p_w^t the pore water pressure.

The water mass balance equation reads in a weak form:

$$\int_{\Omega^t} \left(\dot{M}^t p_w^* - m_i^t \frac{\partial p_w^*}{\partial x_i^t} \right) d\Omega^t = \int_{\Omega^t} Q^t p_w^* \, d\Omega^t - \int_{\Gamma_q^t} \bar{q}^t p_w^* \, d\Gamma^t \tag{11}$$

where $p_w{}^*$ is the virtual pore water pressure field, Q^t is a sink term and Γ_q^t is the part of the boundary where the input water mass per unit area $\bar{q}^t$ is prescribed. M^t and m_i^t are, respectively, the mass of the water inside the current configuration of the skeleton Ω^t and the mass flow.

The mass flow m_i^t is defined as follows:

$$m_i^t = -\rho_w \frac{k_{ij}}{\mu_w} \left[\frac{\partial p_w}{\partial x_j} + \rho_w g_j \right] \tag{12}$$

in which k_{ij} is the anisotropic permeability tensor and μ_w is the water dynamic viscosity.

The compressible fluid is assumed to respect the following relationship, which predicts an increase of water density as a function of the pore water pressure, defining χ_w as the water bulk modulus [28]:

$$\dot{\rho}_w^t = \frac{\rho_w^t}{\chi_w} \dot{p}_w^t \tag{13}$$

If the grains are assumed to be incompressible (which means ρ_s is constant), the time derivative of the water mass is obtained directly by using Eq. (13) and mass balance equation for the solid phase. This yields for a unit mixture volume:

$$\dot{M}^t = \rho_w^t \left[\frac{\dot{p}_w^t}{\chi_w n^t + \frac{\Omega_r^t}{\Omega^t}} \right] \tag{14}$$

For a given boundary value problem at time t, the equilibrium is not a priori met and some residuals appear in the expression of the field Eqs. (9) and (11), which can be rewritten as follows:

$$\int_{\Omega^\tau} \sigma_{ij}^\tau \frac{\partial u_i^*}{\partial x_j^\tau} \, d\Omega^\tau - \int_{\Omega^\tau} (\rho_s(1-\phi^\tau) + \rho_f^\tau \phi^\tau) g_i u_i^* \, d\Omega^\tau - \int_{\Gamma_\sigma^\tau} \bar{t}_i^\tau u_i^* \, d\Gamma^\tau = R^\tau \tag{15}$$

$$\int_{\Omega^\tau} \left(\dot{M}^\tau p_f^* - m_i^\tau \frac{\partial p_f^*}{\partial x_i^\tau} \right) d\Omega^\tau - \int_{\Omega^\tau} Q^\tau p_f^* \, d\Omega^\tau + \int_{\Gamma_q^\tau} \bar{q}^\tau p_f^* \, d\Gamma^\tau = W^\tau \tag{16}$$

where R^τ and W^τ are the mechanical and the flow residuals, respectively.

In order to solve this non-linear problem, a Newton–Raphson scheme is proposed to find a new solution of displacement and pressure fields, for which equilibrium is met. The idea is to define a linear auxiliary problem deriving from the continuum one (instead of the discretized one as it is more usually done) similar to the work of Borja and Alarcon [29]. This approach gives the same results as standard FEM procedure but makes the linearization easier, especially for coupled problem in large strain formulation. In this paper, linearization of balance equations is not fully developed and we refer to [30] for a saturated porous medium with a constant isotropic permeability. The only difference in the linearization procedure comes from the anisotropic permeability tensor, which depends on the displacement field. For that purpose, it is necessary to have the linearization of Eq. (8), which yields:

$$dk_{ij}^t = \sum_l \left(3A_l k_l^0 (1+A_l \varepsilon_l^T)^2 \beta_{ij}^l \frac{\partial \varepsilon_l^T}{\partial \varepsilon_{mn}} + k_l^0 (1+A_l \varepsilon_l^T)^3 \frac{\partial \beta_{ij}^l}{\partial \varepsilon_{mn}} \right) \frac{\partial du_m^t}{\partial x_n^t} = V_{ijmn} \frac{\partial du_m^t}{\partial x_n^t} \tag{17}$$

$$\frac{\partial \varepsilon_l^T}{\partial \varepsilon_{mn}} = \frac{\partial \varepsilon_l^T}{\partial \alpha_l} \frac{\partial \alpha_l}{\partial \varepsilon_{mn}}$$

$$\frac{\partial \beta_{ij}^l}{\partial \varepsilon_{mn}} = \gamma_{ij}^l \frac{\partial \alpha_l}{\partial \varepsilon_{mn}}$$

$$\frac{\partial \alpha_k}{\partial \varepsilon_{mn}} = sign(\alpha_k) \frac{(1-\delta_{mn})(\varepsilon_{11}-\varepsilon_{22}) + (-1)^{m+1} \varepsilon_{12} \delta_{mn}}{(\varepsilon_{11}-\varepsilon_{22})^2 + (2\varepsilon_{12})^2}$$

Following the linearization procedure of the non-linear problem (see [30] for details), the linear auxiliary problem is found and the two corresponding equations are rewritten in a matricial form, in order to define the local element stiffness matrix:

$$\int_{\Omega^t} [U_{(x,y)}^{*,t}]^T [E^t] [dU_{(x,y)}^t] \, d\Omega^t = \int_{\Gamma_q^t} [U_{(x,y)}^{*,t}]^T [F^t] [dU_{(x,y)}^t] \, d\Gamma_q^t - R^t - W^t \tag{18}$$

where $[dU_{(x,y)}^t]$ is defined in Eq. (19) and $[U_{(x,y)}^{*,t}]$ has the same structure as the corresponding virtual quantities:

$$[dU_{(x,y)}^t]^T \equiv \left[\frac{\partial du_1^t}{\partial x_1^t} \frac{\partial du_1^t}{\partial x_2^t} \frac{\partial du_2^t}{\partial x_1^t} \frac{\partial du_2^t}{\partial x_2^t} \; du_1^t \; du_2^t \; \frac{\partial dp_w^t}{\partial x_1^t} \frac{\partial dp_w^t}{\partial x_2^t} \; dp_w^t \right] \tag{19}$$

The finite element spatial discretization is introduced in Eq. (18) using the transformation matrices $[T^t]$ and $[B]$, which connect $[dU_{(x,y)}^t]$ to the nodal variables $[dU_{Node}^t]$. Integration of the left-hand

Please cite this article as: Levasseur S, et al. Hydro-mechanical modelling of the excavation damaged zone around an underground excavation at Mont Terri Rock Laboratory. Int J Rock Mech Mining Sci (2010), doi:10.1016/j.ijrmms.2010.01.006

term of Eq. (18) on a finite element yields:

$$[U^*_{node}]^T \int_{-1}^{1}\int_{-1}^{1} [B]^T[T^t]^T[E^t][T^t][B]\det J^t \, d\xi \, d\eta [dU^t_{Node}] \equiv [U^*_{node}]^T[K^t][dU^t_{Node}] \quad (20)$$

where $[K^t]$ is the local element stiffness matrix, J^t is the Jacobian matrix of the mapping from (ξ,η) to (x,y) for the 2D finite element. $[E^t]$ is a (9×9) matrix that contains all the terms of Eq. (18):

$$[E^t] = \begin{bmatrix} K^t_{MM_{(6\times 6)}} & K^t_{WM_{(6\times 3)}} \\ K^t_{MW_{(3\times 6)}} & K^t_{WW_{(3\times 3)}} \end{bmatrix} \quad (21)$$

Matrices K_{WW} and K_{MM} are the classical stiffness matrices for a flow and a mechanical problem with 2D finite element. K_{WM} and K_{MW} contain all the couplings terms appearing between the mechanical problem and the flow one. The formulation of the different sub-matrices is expressed as follows:

$$K^t_{WW_{(3\times 3)}} = \begin{bmatrix} \rho_w^{\tau 1}\frac{k_{11}}{\mu_w} & \rho_w^{\tau 1}\frac{k_{12}}{\mu_w} & C1 \\ \rho_w^{\tau 1}\frac{k_{21}}{\mu_w} & \rho_w^{\tau 1}\frac{k_{22}}{\mu_w} & C2 \\ 0 & 0 & D \end{bmatrix} \quad (22)$$

$$K^t_{MW_{(3\times 6)}} = \begin{bmatrix} -\rho_w^t\frac{k_{11}}{\mu_w}\frac{\partial p_w^t}{\partial x_1^t}+H_{111} & m_2^t-\rho_w^t\frac{k_{12}}{\mu_w}\frac{\partial p_w^t}{\partial x_1^t}+H_{112} & -\rho_w^t\frac{k_{11}}{\mu_w}\frac{\partial p_w^t}{\partial x_2^t}+H_{121} & -m_1^t-\rho_w^t\frac{k_{12}}{\mu_w}\frac{\partial p_w^t}{\partial x_2^t}+H_{122} & 0 & 0 \\ -m_2^t-\rho_w^t\frac{k_{21}}{\mu_w}\frac{\partial p_w^t}{\partial x_1^t}+H_{211} & -\rho_w^t\frac{k_{22}}{\mu_w}\frac{\partial p_w^t}{\partial x_1^t}+H_{212} & m_1^t-\rho_w^t\frac{k_{21}}{\mu_w}\frac{\partial p_w^t}{\partial x_2^t}+H_{221} & -\rho_w^t\frac{k_{22}}{\mu_w}\frac{\partial p_w^t}{\partial x_2^t}+H_{222} & 0 & 0 \\ N+\dot{M}^t & 0 & 0 & N+\dot{M}^t & 0 & 0 \end{bmatrix} \quad (23)$$

$$K^t_{WM_{(6\times 3)}} = \begin{bmatrix} 0 & 0 & -1 \\ 0 & 0 & 0 \\ 0 & 0 & 0 \\ 0 & 0 & -1 \\ 0 & 0 & -\left(\frac{\rho_w^t}{\chi_w}\phi^t\right)g_1 \\ 0 & 0 & -\left(\frac{\rho_w^t}{\chi_w}\phi^t\right)g_2 \end{bmatrix} \quad (24)$$

where

$$C1 = \frac{\rho_w^t}{\chi_w}\frac{k_{11}}{\mu_w}\left(\frac{\partial p_w^t}{\partial x_1^t}+\rho_w^t g_1\right)+\frac{\rho_w^t}{\chi_w}\frac{k_{12}}{\mu_w}\left(\frac{\partial p_w^t}{\partial x_2^t}+\rho_w^t g_2\right) + \rho_w^t\frac{\rho_w^t}{\chi_w}\frac{k_{11}}{\mu_w}g_1+\rho_w^t\frac{\rho_w^t}{\chi_w}\frac{k_{12}}{\mu_w}g_2 \quad (25)$$

$$C2 = \frac{\rho_w^t}{\chi_w}\frac{k_{21}}{\mu_w}\left(\frac{\partial p_w^t}{\partial x_1^t}+\rho_w^{\tau 1} g_1\right)+\frac{\rho_w^{\tau 1}}{\chi_w}\frac{k_{22}}{\mu_w}\left(\frac{\partial p_w^{\tau 1}}{\partial x_2^{\tau 1}}+\rho_w^{\tau 1} g_2\right) + \rho_w^{\tau 1}\frac{\rho_w^{\tau 1}}{\chi_w}\frac{k_{21}}{\mu_w}g_1+\rho_w^{\tau 1}\frac{\rho_w^{\tau 1}}{\chi_w}\frac{k_{22}}{\mu_w}g_2 \quad (26)$$

$$H_{1mn} = -\rho_w^t\frac{V^t_{11mn}}{\mu_w}\left(\frac{\partial p_w^t}{\partial x_1^t}+\rho_w^t g_1\right)-\rho_w^t\frac{V^t_{12mn}}{\mu_w}\left(\frac{\partial p_w^t}{\partial x_2^t}+\rho_w^t g_2\right) \quad (27)$$

$$H_{2mn} = -\rho_w^t\frac{V^t_{21mn}}{\mu_f}\left(\frac{\partial p_w^t}{\partial x_1^t}+\rho_w^t g_1\right)-\rho_w^t\frac{V^t_{22mn}}{\mu_w}\left(\frac{\partial p_w^t}{\partial x_2^t}+\rho_w^t g_2\right) \quad (28)$$

Note that K_{MW} and K_{WM} are different, resulting in an asymmetry of the coupling matrix. The formulation of the K_{MM} matrix and the expression of D and N can be found in [30].

4. Numerical modelling of dilatometer experiment

Experimental results of the Selfrac project show that the hydraulic conductivity of the EDZ is a function of the inflation pressure of the dilatometer. This is of course a crucial issue to ensure the sealing function to swelling bentonite plugs in nuclear waste repositories. The numerical models have to tackle such a phenomenon, in order to be able to predict the behaviour of the engineer barrier system and to propose a design of the structure. After the development of the constitutive model in Section 3, the aim of this numerical part is to check the capacity of our finite element code to reproduce first qualitatively the experimental results: decrease of the permeability as of function of the dilatometer load. In a second step, we compare also quantitatively the experimental and numerical results in order to evaluate the ability of our model to catch the order of magnitude of the different phenomena.

4.1. Assumptions

Selfrac experiment is drilled perpendicular to the main gallery of the Mont Terri URL, in horizontal plane (Fig. 1a). According to the anisotropic in situ stress field orientation defined by Yong et al. [14] and Corkum and Martin [15], the sub-vertical maximum principal stress is σ_1=6.5 MPa, and the sub-horizontal minimal principal stresses are σ_2=4 MPa (in perpendicular direction of Selfrac borehole) and σ_3=2.2 MPa (in parallel direction of Selfrac borehole). Pore water pressure p_w is equal to 2 MPa. To model the long-term dilatometer experiment, we propose a 2D-axisymetrical finite element model, on which Opalinus Clay anisotropy is neglected compared to the anisotropy of permeability tensor induced by borehole drilling. Clay is idealized to an isotropic medium in isothermal conditions submitted to the vertical principal stress σ_1. The 2D-axisymetrical finite element model associated with this experiment is presented in Fig. 5.

The two main steps of the modelling are the excavation and long-term dilatometer test. During the borehole drilling, the total stress and the pore pressure are decreased down to zero at the borehole wall. During the dilatometer test, the boundary condition at the dilatometer probe and the packer corresponds to an impervious condition for the flow problem and the imposition of the dilatometer total pressure. During this second step, the two intervals are modelled by a highly deformable porous medium with a high permeability value. For the modelling, the Opalinus Clay is supposed to be saturated. During the experimental procedure, the dilatometer pressure increases step by step and is followed by hydraulic tests. As described in Section 2, experiment results show that each hydraulic test performed for dilatometer load lower than 3.5 MPa is only used to test the contact between the dilatometer probe and the host rock. These parts of the experiment before 3.5 MPa of dilatometer load are not considered in this analysis and our modelling is restricted to the calculation phases listed in Table 1.

The Opalinus Clay behaviour is modelled by an elasto-plastic frictional model with a Van Eekelen criterion [31], which consists of a smoothed Mohr–Coulomb plasticity surface. This formulation can be written in a very similar way to

Please cite this article as: Levasseur S, et al. Hydro-mechanical modelling of the excavation damaged zone around an underground excavation at Mont Terri Rock Laboratory. Int J Rock Mech Mining Sci (2010), doi:10.1016/j.ijrmms.2010.01.006

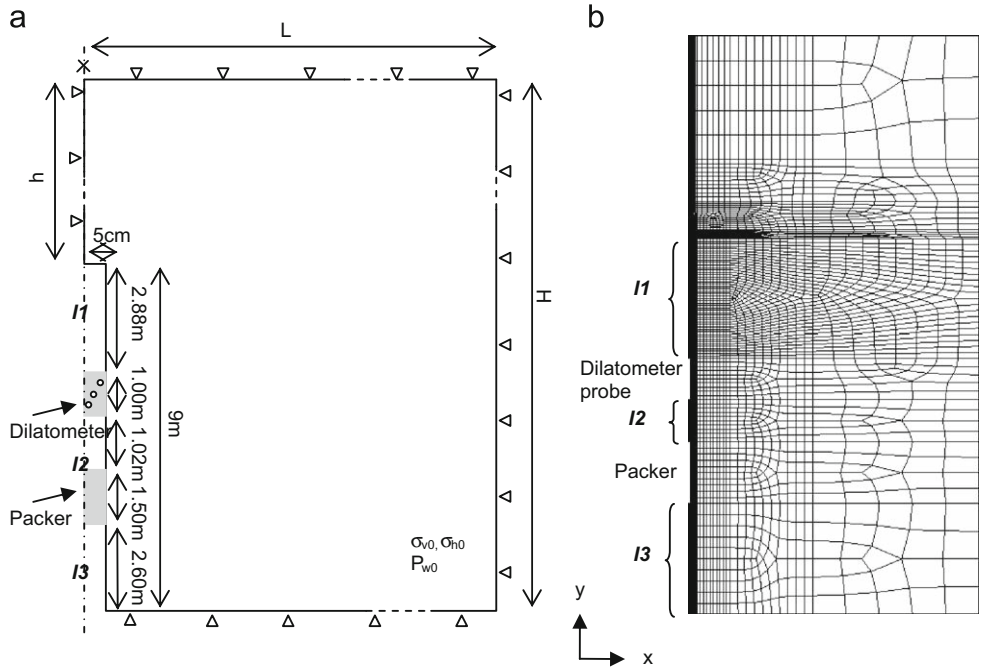

Fig. 5. (a) Axisymmetric schematic representation of Mont Terri dilatometer test and (b) associated 2D-axisymetric finite element model (8-node element type; 4626 elements; 13,795 Nodes)—performed with Lagamine code.

Table 2
Mechanical parameters of non-associated Van Eeckelen criterion and hydraulic parameters in drained conditions for Opalinus Clay [16].

Mechanical characteristics		Hydraulic characteristics	
Young elastic modulus, E_0	10 GPa	Initial porosity, ϕ_0	0.137
Poisson ratio, υ	0.270	Initial intrinsic permeability, k_0^{int}	2×10^{-20} m^2
Specific mass, ρ	2450 kg/m^3	Water specific mass, ρ_f	1000 kg/m^3
Initial cohesion, c'	2 200 kPa	Fluid dynamic viscosity, μ_f	10^{-3} Pa s
Initial friction angle, ϕ_c'	25.0°	Liquid compressibility coefficient, $1/\chi_f$	5×10^{-4} MPa^{-1}
Dilatation angle, ψ	0°		
Biot's coefficient, b	1		

Drucker–Prager's criterion:

$$f = II_{\hat{\sigma}} + m\left(I_\sigma - \frac{3c}{\tan\phi_C}\right) = 0 \tag{29}$$

where $I_\sigma = \sigma_{ii}$ is the first stress tensor invariant, $II_{\hat{\sigma}} = [(\hat{\sigma}_{ij}\hat{\sigma}_{ij})/2]^{1/2}$ is the second deviatoric stress tensor invariant, and $III_{\hat{\sigma}} = \hat{\sigma}_{ij}\hat{\sigma}_{jk}\hat{\sigma}_{ki}/3$ is the third deviatoric stress tensor invariant. A dependence on the third invariant stress is introduced in the model using the parameter m. The shape of the surface in the deviatoric plane is not a circle anymore and extension strength is better evaluated than with the Drucker–Prager's criterion. The coefficient m is defined by

$$m = a(1 + b\sin 3\beta)^n \tag{30}$$

$$\beta = -\frac{1}{3}\sin^{-1}\left(3\frac{\sqrt{3}}{2}\frac{III_{\hat{\sigma}}}{II_{\hat{\sigma}}^3}\right) \tag{31}$$

The Lode angle β is derived from equation of the third invariant and the three parameters a, b and n must verify different convexity conditions [31]. The non-associated and drained parameters of this model, estimated from laboratory and in situ tests [16,32,33], are presented in Table 2.

The weight coefficient A of Eq. (8) related to the coupling between permeability and strain is not directly known. This coefficient, which characterized the micro-structural properties of the medium, is obtained by trial and error in order to match the experimental measurement of transmissivity during the borehole drilling. Because of the hypothesis of isotropic medium, the whole cracks are assumed to have the same properties in average. Experimental results have shown that borehole drilling

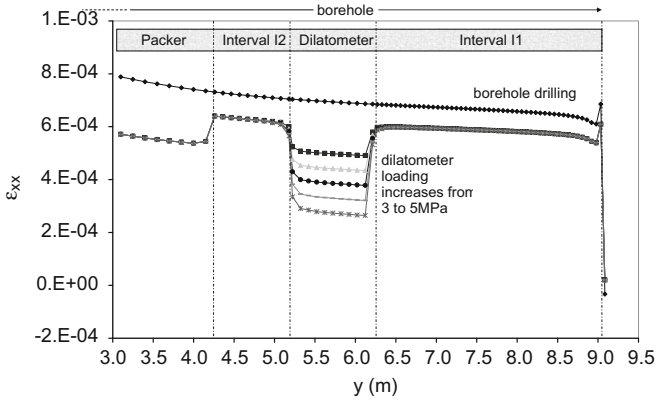

Fig. 6. Radial strains along the borehole after the borehole drilling and for different dilatometer load values (with mechanical convention—positive stains correspond to tensile strains).

sparks off a modification of around five orders of magnitude on axial hydraulic conductivity and quite no modification on radial hydraulic conductivity compare to undisturbed Opalinus Clay [19]. To obtain this degree of modification in numerical predictions, calibration process provides a coefficient A equal to 6×10^4.

4.2. Numerical results

The first step of this modelling is the borehole drilling. Fig. 6 shows that the borehole drilling induces the development of tensile strains within the excavated damaged zone. As a consequence, permeability tensor in EDZ becomes anisotropic as shown in Fig. 7, which represents the radial and axial permeability components.

During the second step of modelling, the dilatometer and the packer are installed in the borehole and their pressure increases to 3 MPa. This operation has a direct impact on the radial strains (Fig. 6) and the axial conductivity (Fig. 7a): the tensile strains decrease and the axial permeability is reduced especially near the dilatometer. The effect of the dilatometer loads cannot be noticed in such amplitude in other part of the borehole.

Permeability values in situ obtained within the sidewall of the borehole vary considerably and seem to depend on fracture density and interconnectivity [20]. Experimental observations show the presence of three zones around the borehole, in which unloading fractures are oriented parallel to the tunnel walls:

(a) The inner zone or "damaged zone" in which a high fracture density and an initial local permeability increase of up to several orders of magnitude and the fracture density decreases with distance. According to Bossart et al. [20], this zone contains induced fractures caused by high deviatoric stresses close to tunnel wall and is characterized mainly by extensional failure parallel to the tunnel wall and reactivated bedding planes. This zone in Opalinus Clay at Mont Terri Rock Laboratory is supposed to extend for 0.5–1 tunnel radii from the excavation periphery [17,20]. In our case, it corresponds to around 5 cm.

(b) The outer zone or "disturbed zone" in which only reversible changes are observed. Micro-fracturing does not lead to a significant alteration of the flow and transport properties. The permeability in this zone is quite similar to the intact rock.

(c) The intact rock where no construction induced change is observed and the permeability is in its undisturbed state.

The size of the disturbed/damaged zone can be characterized by two variables: the plastic indicator, or the distance on which axial permeability significantly changes. Figs. 8 and 9 show the evolution of the plastic indicator and the axial permeability values along sections perpendicular to the borehole in mid-section of I1 and in mid-section of the dilatometer probe. Note that the plastic indicator is a reduced deviator equal to 1 if the current state is elasto-plastic (on the yield limit) and less than 1 otherwise (elastic behaviour). According to Fig. 8a, axial permeability is strongly modified on the first 10 cm behind the borehole; from 10 to 30 cm from the borehole its evolution is less important; at a radial distance larger than 30 cm axial permeability is quite constant. According to Fig. 8b, plastic indicator is equal to 1 (plastic zone) just behind the borehole and is half-reduced on the first 5 cm behind the borehole; at larger radial distance plastic indicator evolution is not anymore significant. Furthermore, we

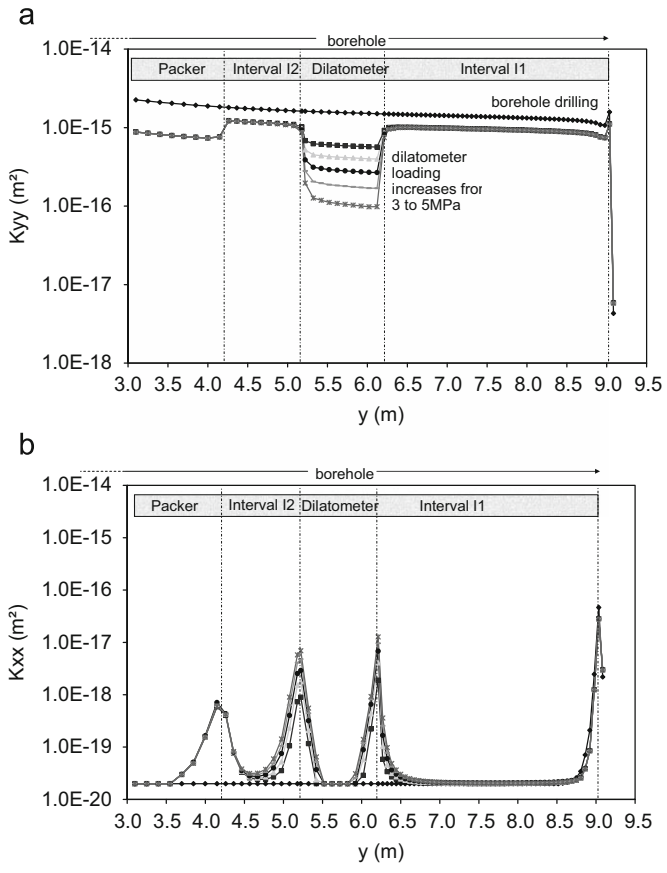

Fig. 7. Permeability along the borehole after the borehole drilling and for different dilatometer loads: (a) axial K_{yy} and (b) radial K_{xx}.

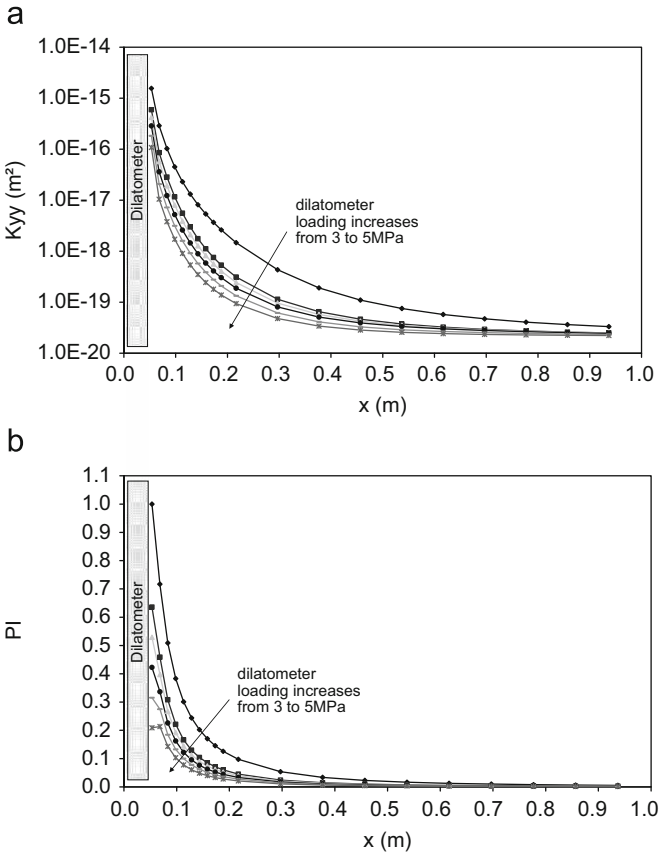

Fig. 8. Section perpendicular to the borehole in mid-length of the dilatometer probe after the borehole drilling and for the different dilatometer loads: (a) axial K_{yy} and (b) plastic indicator PI.

Please cite this article as: Levasseur S, et al. Hydro-mechanical modelling of the excavation damaged zone around an underground excavation at Mont Terri Rock Laboratory. Int J Rock Mech Mining Sci (2010), doi:10.1016/j.ijrmms.2010.01.006

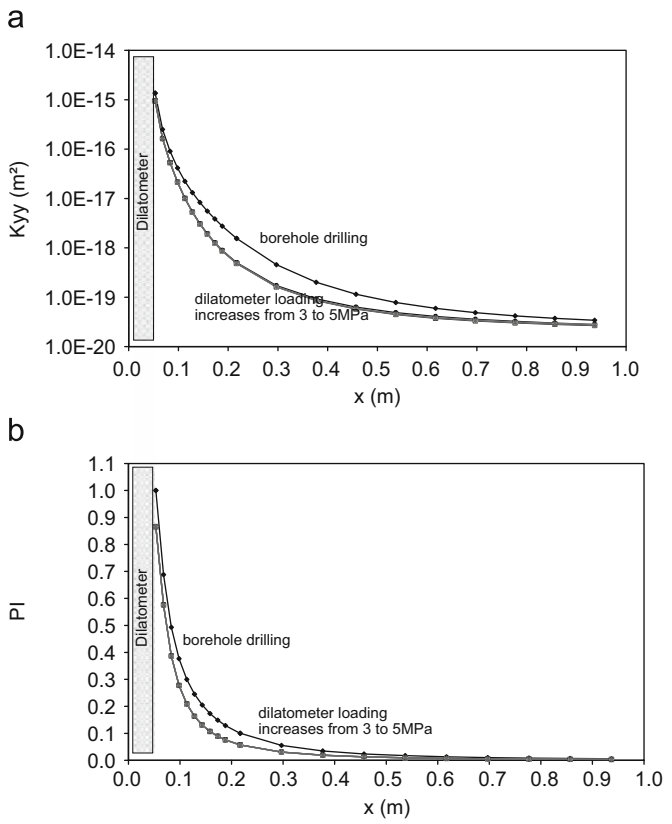

Fig. 9. Section perpendicular to the borehole in mid-length of I1 after the borehole drilling and for the different dilatometer loads: (a) axial K_{yy} and (b) plastic indicator PI.

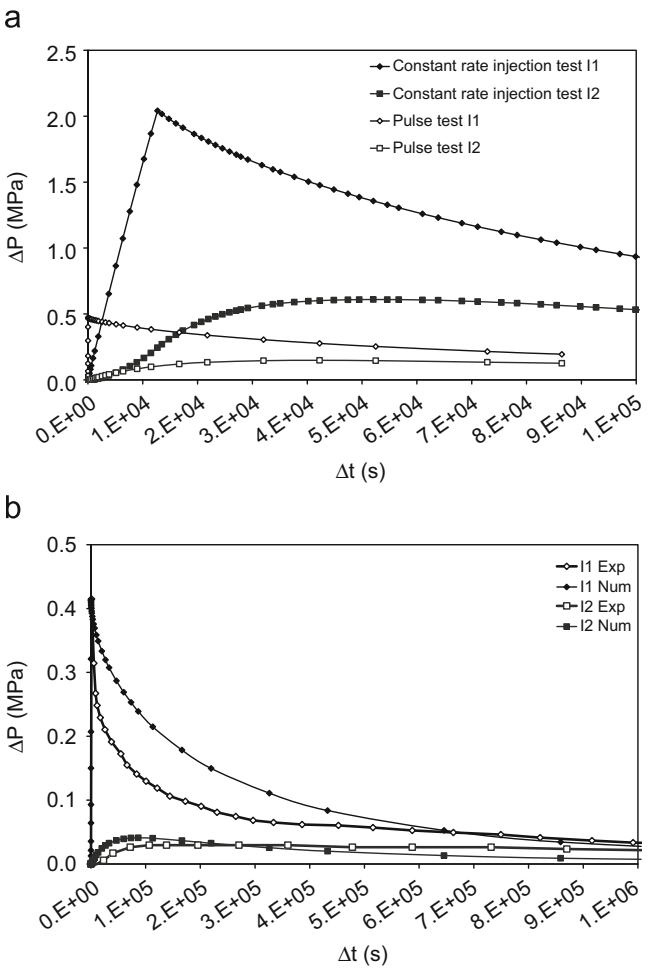

Fig. 10. (a) Temporal evolution of the pressure in I1 and I2 intervals during the first constant rate injection test and during the first pulse injection ($P_{dilatometer}$=3 MPa) and (b) comparison between experimental data and numerical results for the last pulse test ($P_{dilatometer}$=5 MPa).

can notice on these graphs that dilatometer loadings reduce the permeability and the plastic indicator behind the dilatometer probe (Fig. 8) but have no effect on them behind I1 interval (Fig. 9). It means that EDZ size is directly link to dilatometer loading. Moreover, based on plastic indicator evolution, EDZ size evaluated numerically can be considered in agreement with experiment, whereas that based on axial permeability evolution, EDZ size is overestimated. This overestimation could be explained by the definition of permeability tensor with tensile strains, which depends on both elastic and plastic stains. In fact, the whole elastic zone does not participate in the creation of EDZ. But considering only plastic and yielded zones (PI=1) do not either permit to well estimate EDZ size. EDZ is different than plastic and yielded zone [1] then its size is underestimated by a criterion based on the plastic indicator equal to one. To well estimate EDZ size it will be necessary in the future to modify permeability tensor definition in order to consider plastic zone and one part of elastic zone. According to the results presented in Figs. 8 and 9, considering strains associated to a half-reduction of the plastic indicator seems to be a first lead to go on this way.

During the third step, hydraulic tests are performed from I1 interval (Table 1). The first hydraulic test is a constant rate injection test: water is injected (constant flow equals to 83 ml/min) in I1 during several hours. Fig. 10a shows that the pressure in I1 first increases and this overpressure progressively diffuses into the host rock. As permeability is larger in the direction parallel to the borehole than in the radial direction, the water flows out along the dilatometer to finally reach I2 interval and the pressure in I2 increases. This first hydraulic test is followed by a pulse injection test: 39 ml of water is injected during 35 s. Due to the quick injection, the pressure in I1 fast increases, compare to the previous hydraulic test, and the water flows out along the dilatometer. Moreover, even if the injection time is small, it imposes an increase of the pressure in I2. The following phases of this modelling consist to alternate increasing of dilatometer load with hydraulic tests. For each phase, the dilatometer load is increased by step of 0.5 MPa in order to reach 5 MPa at the end of the experiment. The next hydraulic tests are one constant rate injection test and four pulse withdrawal tests as described in Table 1. Compare to measurements of pore pressure in I1 and I2, we can see in Fig. 10b, drawn for the last pulse test performed at 5 MPa of dilatometer pressure, that pressure evolutions follow similar tendencies. The magnitude of pressure is well estimated and the maximum of pressure in I1 and I2 are obtained at quite the same time in the experiment as in the numerical model. However, it is important to notice that for lower dilatometer pressure, the numerical model can sometimes slightly overestimate pressures in I1 and underestimate pressures in I2. Fig. 3 compares the ratio of water overpressures in I1 and I2 measured during the experiment and obtained numerically. Polynomial tendency curves on these data show that a good agreement between experiment and modelling is obtained as far as the dilatometer loading increase. But, for weak dilatometer load, the numerical ratio P_{w1}/P_{w2} overestimates experimental measurements. These differences could be explained by residual flows along the dilatometer probe in contact between soil and dilatometer probe at the beginning of the experiment (inexistent in the model), or by anisotropic properties of the Opalinus Clay

Please cite this article as: Levasseur S, et al. Hydro-mechanical modelling of the excavation damaged zone around an underground excavation at Mont Terri Rock Laboratory. Int J Rock Mech Mining Sci (2010), doi:10.1016/j.ijrmms.2010.01.006

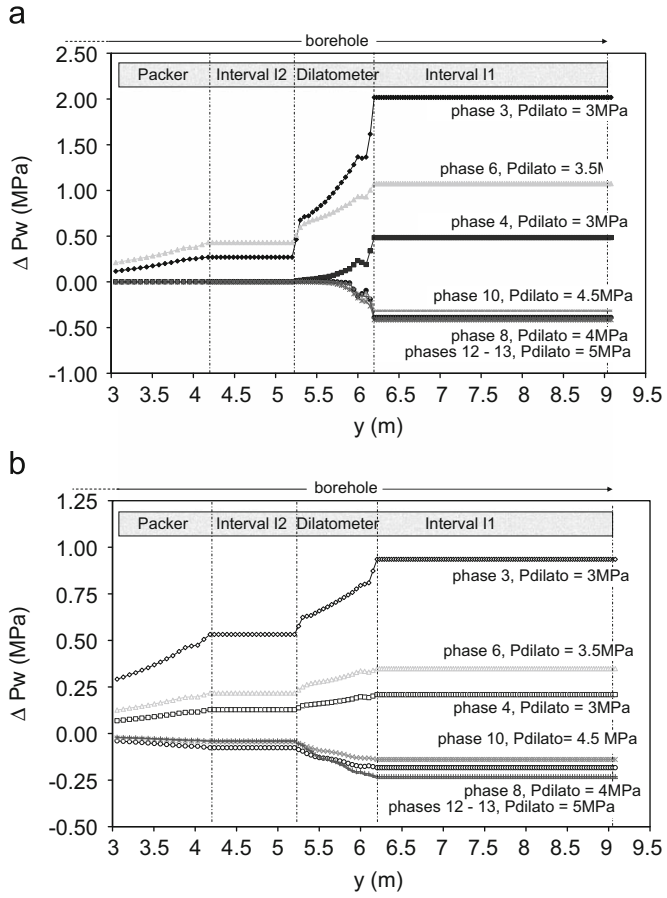

Fig. 11. Water pressure (a) along the borehole at the end of each hydraulic test (a), and (b) 24 h later.

(in situ anisotropy allows more diffusion in the borehole plane than the isotropic model does). It means that the link between transmissivity evolution and inflation pressure of the dilatometer can be reproduced in this model but could also be improved in further developments by anisotropic considerations.

To go ahead in our analysis, Figs. 7a and 8a summarize, respectively, the evolution of the axial permeability after each dilatometer loading along the borehole and in a section perpendicular to the borehole (at the mid-length of the dilatometer probe). We observe that the axial permeability value near the dilatometer is influenced by the dilatometer load. More the dilatometer load increases, more the permeability decreases. This means that from a given load, the two intervals will be hydraulically uncoupled. We can also notice that the hydraulic tests have no influence on the permeability tensor: water flows out within the EDZ without modifying its characteristics.

Fig. 11 summarizes the water pressure evolution along the borehole at the end of each hydraulic test and 24 h later. Fig. 12 presents the overpressure evolution in I2 interval after each pulse test. Fig. 11a shows that each hydraulic test obviously induces a modification of the water pressure in I1 interval. Fig. 11b shows that these overpressures in I1 are followed by modifications of the water pressure in I2 interval. However, we can distinguish different cases:

(a) for dilatometer loads equal to 3 and 3.5 MPa, the injection tests quickly induce a high pressure increase in I2 interval: water still flows out from I1 to I2 through the EDZ (Fig. 11a). The numerical predictions show that the conclusions are the same for the withdrawal test at 4 MPa.

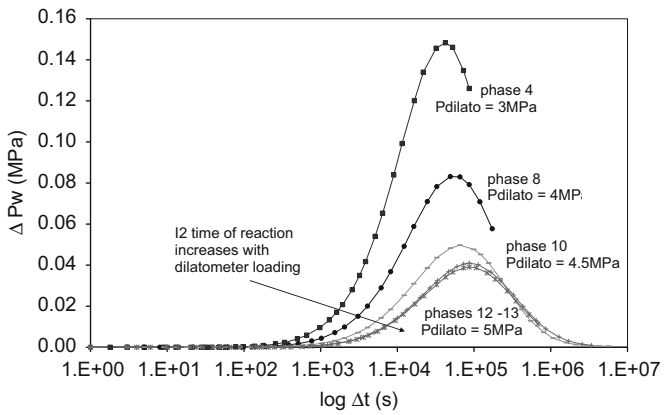

Fig. 12. Numerical results on I2 pressure reaction to pulse test with dilatometer load versus time.

(b) when the dilatometer load is larger than 4 MPa, the water pressure in I2 interval is not significantly modified anymore: overpressure in I2 is weak, the two intervals are not hydraulically coupled through the EDZ anymore.

These results show that, like in the experiment, the dilatometer load has an influence on the water flow. Higher is the dilatometer load, smaller is the water flow from I1 to I2. The threshold dilatometer value is estimated in the vicinity of 4 MPa from the numerical model, and in the vicinity of 3.5 MPa from experimental results. Knowing that the dilatometer loading is performed step by step with increments of 0.5 MPa, we could consider that numerical and experimental results are in agreement. The effect of the dilatometer load can also be evidenced in another way: it needs a time delay for the pressure pulse in interval 1 to reach the neighbouring interval. Experimentally, it has been demonstrated that the delay of this pressure reaction in interval 2 depends on the applied load onto the borehole wall [13]. Fig. 12 shows that the proposed numerical model reproduces this effect: the higher the dilatometer load, the later the overpressure in I2. The dilatometer load delays the pressure reaction in the adjacent test interval I2. Then, all these results show how this modelling well characterizes the dependence between transmissivity and dilatometer loads.

5. Conclusion

Low permeability is one characteristic expected for the geological formation of an underground nuclear waste disposal. All the processes altering this property should therefore be forecast and controlled. The excavation damaged zone is a phenomenon that occurs in the most rock masses as a consequence of underground excavation. The EDZ appears as an area around the underground openings, where geotechnical and hydro-geological properties are altered. The numerical model should be able to predict the evolution of the permeability in the EDZ, in order to permit a well adapted design of technical barriers and seals.

This paper presents first an in situ test that evaluates the permeability changes occurring within the EDZ and more specifically it studies the influence of bentonite swelling pressure on the axial transmissivity of an excavation damaged zone in the Opalinus Clay. The general concept of this experiment is to combine a long-term dilatometer test and numerous hydraulic tests with multi-packer system. The pressure in the dilatometer probe is increased stepwise and hydraulic tests are periodically

Please cite this article as: Levasseur S, et al. Hydro-mechanical modelling of the excavation damaged zone around an underground excavation at Mont Terri Rock Laboratory. Int J Rock Mech Mining Sci (2010), doi:10.1016/j.ijrmms.2010.01.006

performed under different dilatometer pressures. Active hydraulic tests are carried out periodically in the deepest interval of the borehole. The pressure reactions are observed in the test interval as well as the interval above the dilatometer. Experiment shows that pressure changes are preferably transmitted through the EDZ along the borehole. As a consequence, the hydraulic conductivity of the EDZ is a function of inflation pressure of the dilatometer.

A constitutive model is then proposed to predict the evolution of the permeability within the EDZ. In indurated clay, like Opalinus Clay, EDZ is mainly characterized by extensional fracture and the proposed model relates the conductivity changes to the crack aperture in tensile mode. Using an additional hypothesis on the link between crack opening and the principal strain tensor, our model is able to predict an anisotropic evolution of the permeability tensor during the excavation. Based on the Selfrac long-term dilatometer modelling, we have shown that this approach permits to reproduce behaviours of indurated clays. An EDZ of few centimetres behind the borehole can be identified after the excavation. In this area, a high fracture density exists and is characterized by permeability increases of up to several orders of magnitude. This fracture density decreases with the radial distance. Moreover, when dilatometer pressure increases, the axial permeability decreases. No significant water flow can evolve in EDZ behind the dilatometer. The comparisons between numerical predictions and measurements of the pressures in the intervals exhibit a good agreement and confirm that our model is able to catch the main hydro-mechanical processes occurring within the EDZ in indurated clay. Numerical tendencies in terms of pore water pressure are correct, even if for low dilatometer pressure, water pressure can be overestimated in front of the dilatometer and underestimated behind the dilatometer probe. These differences are partly due to assumptions in the finite element modelling and in the permeability tensor definition. To reduce them, further improvements could be imagined in our approach by considering anisotropic properties and in situ conditions of Opalinus clay through a 3D model, perhaps as proposed in [34], or by another description of cracking through the development of a homogenisation model based on micro-mechanical concepts, such as [8].

Acknowledgements

The authors would like to thank the FRS-FNRS, the national funds of scientific research in Belgium, and the European project TIMODAZ for their financial support. TIMODAZ is cofunded by the European Commission (EC) as part of the sixth Euratom research and training Framework Programme (FP6) on nuclear energy (2006–2010).

References

[1] Tsang CF, Bernier F, Davis C. Geohydromechanical processes in the Excavation Damaged Zone in crystalline rock, rock salt and indurated and plastic clays in the context of radioactive waste disposal. Int J Rock Mech Min Sci 2005;42:109–25.

[2] Bernier F, Li XL, Bastiaens W. 'Twenty-five years' geotechnical observation and testing in the Tertiary Boom Clay formation. Géotechnique 2007;57(2): 229–37.

[3] Blüming P, Konietzky H. Development of an excavation d isturbed zone in claystone. In: Natau O, Fecker S, Pimentel S, editors. Geotechnical measurements and modeling. Lisse: Swets & Zeitlinger; 2003. p. 127–32.

[4] Bernier F, Li XL, Bastiaens W, Ortiz L, Van Geet M, Wouters L, et al. Fractures and Self-healing within the Excavation Disturbed Zone in Clays (SELFRAC). Final report, 5th EURATOM Framework Programme (1998–2002), 2007.

[5] NAGRA. Demonstration of disposal feasibility for spent fuel, vitrified high-level waste and long-lived intermediate-level waste. Project Opalinus Clay, Safety Report. Technical Report 02-05, 2002, 472 pp.

[6] Shao JF, Zhou H, Chau KT. Coupling between anisotropic damage and permeability variation in brittle rocks. Int J Numer Anal Methods Geomech 2005;29:1231–47.

[7] Olsson R, Barton N. An improved model for hydromechanical coupling during shearing of rock joints. Int J Rock Mech Min Sci 2001;38:317–29.

[8] Dormieux L, Kondo D. Approche micromécanique du couplage perméabilité-endommagement. C R Méc 2004;332:135–40.

[9] Snow DT. Anisotropic permeability of fractured media. Water Resour Res 1969;5(6):1273–89.

[10] Witherspoon PA, Wang JSY, Iwai K, Gale JE. Validity of cubic law for fluid flow in a deformable rock fracture. Water Resour Res 1980;16(6):1016–24.

[11] Liu J, Elsworth D, Brady BH. Linking stress-dependant effective porosity and hydraulic conductivity fields to RMR. Int J Rock Mech Min Sci 1999;36: 581–96.

[12] Chen YF, Zhou CB, Sheng Y. Formulation of strain dependant hydraulic conductivity for fractured rock mass. Int J Rock Mech Min Sci 2007; 44:981–96.

[13] Bühler Ch. Selfrac (SE) Experiment: long term dilatometer experiment. Mont Terri Project-Technical Note, TN 99-03, 2005.

[14] Yong S, Loew S, Fiedelibus C, Frank E, Lemy F, Schuster K. Induced fracturing in the Opalinus clay: an integrated field experiment. In: Proceedings of the 4th Asian Rock Mechanics Symposium, 8–10 November 2006, Singapore.

[15] Corkum AG, Martin CD. The mechanical behaviour of weak mudstone (Opalinus Clay) at low stresses. Int J Rock Mech Min Sci 2007;44:196–209.

[16] Bock H. Rock mechanics analyses and synthesis (RA experiment): data report on rock mechanics. Mont Terri Technical Report 2000–02, 2001, 52 pp.

[17] Yong S, Keiser PK, Loew S, Fidelibus C. The role of heterogeneity on the development of excavation-induced fractures in Opalinus clay. In: Proceedings of the 61st Canadian Geotechnical Conference, 21–24 September 2008, Edmonton, Canada.

[18] Alheid HJ, Aranyossy JF, Blüming P, Hoteit N, Van Geet M. EDZ development and evolution: state of the art report. NF-Pro project, 6th EURATOM Framework Programme, 2005.

[19] Bossart P, Trick Th, Meier PM, Mayor JC. Structural and hydrogeological characterisation of the excavation disturbed zone in Opalinus Clay (Mont Terri Project, Switzerland). Appl Clay Sci 2004;26:429–48.

[20] Bossart P, Meier PM, Moeri A, Trick Th, Mayor JC. Geological and hydraulic characterization of the excavation disturbed zone in the Opalinus Clay of the Mont Terri Rock Laboratory. Eng Geol 2002;66:19–38.

[21] Oda M. Permeability tensor for discontinuous rock masses. Geotechnique 1985;35(4):483–95.

[22] Indraratna B, Ranjith P. Hydromechanical aspects and unsaturated flow in jointed rock. Rotterdam: Balkema; 2001.

[23] Zangerl C, Evans KF, Eberhardt E, Loew S. Normal stiffness of fractures in granite rock: a compilation of laboratory and in situ experiments. Int J Rock Mech Min Sci 2008;45:1500–7.

[24] Marache A, Riss J, Gentier S. Experimental and modelled mechanical behaviour of a rock fracture under normal stress. Rock Mech Rock Eng 2008; 41:869–92.

[25] Olsson R, Barton N. An improved model for hydromechanical coupling during shearing of rock joints. Int J Rock Mech Min Sci 2001;38:317–29.

[26] Giacomini A, Buzzi O, Ferrero AM, Migliazza M, Giani GP. Numerical study of flow anisotropy within a single natural rock joint. Int J Rock Mech Min Sci 2008;45:47–58.

[27] Zhou CB, Sharma RS, Chen YF, Rong G. Flow-stress coupled permeability tensor for fractured rock masses. Int J Numer Anal Methods Geomech 2008; 32(11):1289–309.

[28] Lewis RW, Schrefler BA. The finite element method in the static and dynamic deformation and consolidation of porous media. New York: Wiley; 2000.

[29] Borja R, Alarcon E. A mathematical framework for finite strain elastoplastic consolidation. Part 1: balance law, variational formulation and linearization. Comput Methods Appl Mech Eng 1995;122:765–81.

[30] Collin F, Chambon R, Charlier R. A finite element method for poro-mechanical modelling of geotechnical problems using local second gradient models. Int J Numer Methods Eng 2006;65(11):1749–72.

[31] Van Eekelen HAM. Isotropic yield surfaces in three dimensions for use in soil mechanics. Int J Numer Anal Methods Geomech 1980;4:98–101.

[32] Coll C. Endommagement des roches argileuses et perméabilité induite au voisinage d'ouvrages souterrains. PhD thesis, Univ Joseph Fourier, 2005.

[33] Martin CD, Lanyon GW. Measurement of in situ stress in weak rocks at Mont Terri Rock Laboratory, Switzerland. Int J Rock Mech Min Sci 2003; 40:1077–88.

[34] Chen L, Shao JF, Huang HW. Coupled elastoplastic damage modelling of anisotropic rocks. Comput Geotech 2009, doi:10.1016/j.compgeo.2009.09.001.

Please cite this article as: Levasseur S, et al. Hydro-mechanical modelling of the excavation damaged zone around an underground excavation at Mont Terri Rock Laboratory. Int J Rock Mech Mining Sci (2010), doi:10.1016/j.ijrmms.2010.01.006